Coastal and mesoscale dynamics characterization using altimetry and gliders: A case study in the Balearic Sea

Jérôme Bouffard,[1] Ananda Pascual,[1] Simón Ruiz,[1] Yannice Faugère,[2] and Joaquín Tintoré[1,3]

Received 29 December 2009; revised 9 June 2010; accepted 21 June 2010; published 13 October 2010.

[1] Dynamics along the continental slopes are difficult to observe given the wide spectrum of temporal and spatial variability of physical processes which occur (coastal currents, meanders, eddies, etc.). Studying such complex dynamics requires the development of synergic approaches that use integrated observing systems. In this context, we present the results of an observational program conducted in the Balearic Sea combining coastal gliders and altimetry. The objectives of this experiment are to study regional dynamics using new technologies, such as gliders, in synergy with satellite altimetry and to investigate the limitations and potential improvement to altimetric data sets in the coastal zone. In this regard, new methodologies have been developed to compute consistent altimetric and glider velocities, and a novel technique to estimate absolute glider velocities, combining surface glider geostrophic velocities with integrated currents estimated from the glider GPS positioning, has been applied. In addition, the altimetric velocity computation has been improved, especially in the coastal zone, using high-frequency along-track sampling associated with new filtering and editing techniques. This approach proves efficient for homogenizing the physical contents of altimetry and glider surface currents (percentage of standard deviation explained is >40) and characterizing regional dynamics in the Balearic Sea through a combined analysis of a high-resolution observing system, such as the appearance of anomalous intense mesoscale features missing in the classical circulation scheme of the Balearic Sea.

Citation: Bouffard, J., A. Pascual, S. Ruiz, Y. Faugère, and J. Tintoré (2010), Coastal and mesoscale dynamics characterization using altimetry and gliders: A case study in the Balearic Sea, *J. Geophys. Res.*, *115*, C10029, doi:10.1029/2009JC006087.

1. Introduction

[2] New monitoring technologies are being progressively implemented in coastal ocean observatories, increasing our understanding of coastal and nearshore processes and contributing to a more science based and sustainable management of the coastal area.

[3] By autonomously collecting high-quality observations in three dimensions, gliders allow high-resolution oceanographic monitoring and provide useful contributions to the understanding of mesoscale dynamics [e.g., *Hodges and Fratantoni*, 2009; *Ruiz et al.*, 2009a] and multidisciplinary interactions that significantly affect upper ocean biogeochemical exchanges, an issue of worldwide relevance in the context of climate change. However, isolated measurements from fleets of gliders are not sufficient as, for many processes, glider measurements remain scarce, both in space and time. Instead, a multisensor approach that combines in situ and remote-sensing measurements should provide a better understanding of observed features, especially through an increase of space-time coverage. This is one of the key conclusions and recommendations reached during the recent OceanObs09 Conference.

[4] To properly address the new scientific challenges associated with the coastal marine variability (including physical, biogeochemical, and ecosystem variations), an intensive observational program has been conducted in the Balearic Sea (western Mediterranean), in particular aiming at combining coastal glider and satellite altimetry data. The physical content of the two data sets and their potential synergy and limitations in the coastal domain have been explored. Four glider missions have been used, carried out from July 2007 to June 2008. These missions were approximately simultaneous and well colocalized with Envisat satellite passages whose measurements are almost perpendicular to the main Balearic oceanographic features (see Figure 1). The Balearic subbasin is a region of worldwide interest characterized by both permanent and variable signals, covering a wide range of dynamical scales from intense mesoscale (in terms of filaments, eddies, or shelf-slope flow modifications) to seasonal and interannual variability. The main Balearic

[1]Marine Technologies, Operational Oceanography, and Sustainability Department, Mediterranean Institute for Advanced Studies, Mallorca, Spain.
[2]CLS Space Oceanography Division, Ramonville, France.
[3]Also at Balearic Islands Coastal Observatory System, Mallorca, Spain.

Copyright 2010 by the American Geophysical Union.
0148-0227/10/2009JC006087

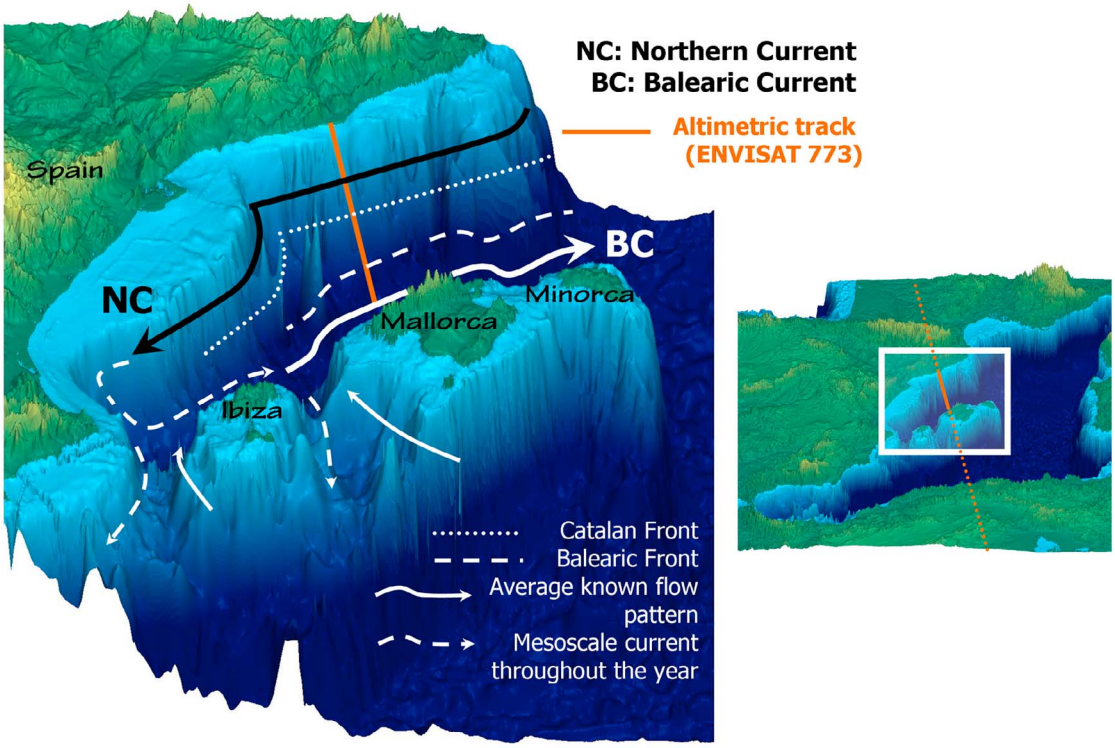

Figure 1. Location of Envisat track 773, bathymetry and main surface circulation characteristics of the Balearic subbasin (western Mediterranean) [modified from *Pascual et al.*, 2004].

oceanographic features share the results of process interactions at basin, subbasin, and local scales. Thermohaline adjustments take place over the western Mediterranean Sea and govern the eastward and northeastward spreading of Atlantic Water (AW) inflowing through Gibraltar Strait. This flow can reach the Balearic Islands, therefore influencing north and south heat transport and exchanges that appear to have key relevance to upper level ecosystem variability and fisheries.

[5] The general surface circulation of the Balearic Sea is controlled by the presence of two fronts and their associated currents [*Font et al.*, 1988; *Font*, 1990; *Pinot et al.*, 1994; *Onken et al.*, 2008]. The Catalan front is a shelf-slope front that separates old AW, in the centre of the Balearic subbasin, from the less dense water transported by the Northern Current (NC), which is also old AW but is fed into the Gulf of Lions and the Catalan shelves by fresh continental water. The NC flows southwestward along the continental slope until it either exits the basin through the Ibiza Channel, or retroflects cyclonically over the insular slope forming the Balearic Current (BC; see Figure 1). The BC is also fed by recent warm and fresh AW waters coming from the Algerian Basin through the Mallorca and Ibiza channels. Both the Northern and Balearic currents have widths of the order of 50 km and are in good geostrophic balance, as winds only seem to produce transient perturbations in near-inertial oscillations [*Font*, 1990]. In addition to the general basin scale circulation, the Balearic subbasin is also characterized by frontal dynamics near the slope areas: Mesoscale eddies [*Tintoré et al.*, 1990; *Pinot et al.*, 2002; *Rubio et al.*, 2009] as well as filaments and shelf-slope flow modifications [*La Violette et al.*, 1990] have been found to modify, not only the local dynamics (significant vertical motion associated [*Pascual et al.*, 2004]), but also the large scale patterns, as shown by *Pascual et al.* [2002] in a detailed study of the blocking effect of a large anti-cyclonic eddy, as well as showing a clear influence of basin circulation on phytoplankton biomass [*Jordi et al.*, 2009]. Seasonal frequency observations of the NC [*Béthoux*, 1980; *Font et al.*, 1988] reveal higher transports in winter than in summer (1.5–2 Sv and 1 Sv, respectively), while the opposite is found in the BC (0.3 Sv in winter compared with 0.6 Sv in summer). Regarding interannual variability, a recent study with along-track satellite altimetry [*Birol et al.*, 2010], has shown large year-to-year differences, suggesting complex non-linear interactions between basin scale and mesoscale circulations.

[6] Several previous studies at the Balearic subbasin scale have been done, however most were from observational cruises carried out on the mainland side and focused on the NC or on the exchanges of water through the Balearic channels; few experiments have been devoted to study the BC and its associated front. In a recent work, *Ruiz et al.* [2009b] provided the first positive insights concerning the use of gliders in synergy with altimetry in order to monitor dynamics in semi-enclosed basins such as the Balearic area. That paper showed reasonable qualitative agreements between absolute dynamic topography (ADT) from altimetry and dynamic height (DH) derived from glider measurements. However, although the first results were encouraging, the study was limited to only two glider missions over a relatively short distance (<90 km) that did not allow robust altimetry-glider velocity comparisons (especially in terms of velocity gra-

Table 1. Altimetric Product Characteristics

Products	Resolution	Spatial Filtering	Editing	Time Sampling
Along-track 1 Hz SLA[c] Envisat track 773	~7 km	20 km[a]	New[b]	35 days Instantaneous
Along-track 20 Hz SLA Envisat track 773	~0.350 km	20 km	New[b]	35 days Instantaneous
Gridded field ((M)SLA)[d] Multimissions	1/8°	>42 km	Standard	7 days Time-averaged

[a]Forty-two kilometers in *Ruiz et al.* [2009a].
[b]See section 3.1.1.
[c]Sea level anomaly, SLA.
[d]Map of sea level anomaly, (M)SLA.

dients in the coastal zone). Moreover, the use of a reference level at 180 m to compute glider $DH_{z_{180}}$ does not appear to totally satisfy the dynamical processes marked by a deep thermocline, such as eddies or coastal currents which might be expected in this area. In addition, some altimetric data near the coast was missing, especially due to land contamination in the altimeter footprint and associated data eliminations. This last issue suggested the need for specific algorithms dedicated to coastal zone applications (e.g., altimetric waveform retracking, dedicated quality control procedure, etc.).

[7] On the basis of these issues, new strategies have been developed within the framework of this study in order to more precisely characterize coastal and mesoscale dynamics in terms of current velocity. The altimetric velocity computation has been improved, especially in the coastal zone, by associating high-frequency along-track sampling to new filtering and editing techniques, and a new methodology has been applied to estimate absolute glider velocities by using velocities derived from glider GPS positions, a complementary and relevant variable not fully exploited in previous studies. Thus, beside the main scientific objective of our study, which consists at characterizing dynamical processes at regional and coastal scales, the two complementary objectives are to investigate limitations and potential improvements to altimetric velocity computation in the coastal area; and to develop and assess methods for future combining of glider and altimetry data sets by homogenizing their physical content.

[8] To give an answer to the questions addressed, this study is organized as follows: After a detailed presentation of the data sets used, we explain the strategies developed to compute homogeneous altimetric and glider surface absolute geostrophic currents (SAGC) with a special emphasis on error budget evaluation. We then provide qualitative and quantitative cross validations between altimetric and glider current velocity through four examples corresponding to characteristic dynamical events associated with the Balearic current dynamical system. Finally, our conclusions are summarized.

2. Data Sets and Variables Used

2.1. Sea Surface Height From Altimetry

[9] Altimetry allows a direct computation of geostrophic velocity anomalies [e.g., *Pascual et al.*, 2009, and references therein]; by adding the geostrophic mean currents derived from a mean dynamic topography (MDT) [*Rio et al.*, 2007], it is then possible to build SAGC. However, conventional altimetry measurements remain largely unusable in the coastal zone [*Anzenhofer et al.*, 1999; *Volkov et al.*, 2007; *Bouffard et al.*, 2010] due to several factors such as inaccurate geophysical corrections (e.g., atmospheric and tidal signals) as well as environmental issues (e.g., land contamination in altimetric and radiometric footprints). At present, new coastal altimeter products are under development (COASTALT, PISTACH, X-TRACK). Several studies show that we can now be confident of such experimental data for scales greater than 20 km and up to 15 km far from the coast [*Vignudelli et al.*, 2005; *Bouffard et al.*, 2008, 2010; *Durand et al.*, 2008, 2010; *Cipollini et al.*, 2010]. The main developments involve the application of coastal-oriented corrections and the review of the data recovery strategies near the coast.

[10] In this paper, we will specifically focus on the impact of filtering and new editing strategies, combined with high-frequency along-track sampling. In this regard, we will use three different altimetric data sets (see Table 1 for altimetric product characteristics): Two along-track data (1 and 20 Hz) and a multisatellite gridded field, the map of sea level anomalies (M)SLA.

2.1.1. Along-Track Data Sets

[11] We used Envisat data sets provided by CLS (Y. Faugère et al., personal communication, 2009) for track 773, cycles 59, 63, 67, and 69 being associated with the dates of passage of the satellite of 8 July 2007, 25 November 2007, 13 April 2008, and 22 June 2008 respectively. These are almost simultaneous with the glider missions; in each case there is a temporal lag of less than 1 week.

[12] The processing of altimeter data used here is similar to the one described in the "Ssalto/Duacs User Handbook" [*Ssalto/Duacs*, 2006]. The only differences were the sampling, editing, and filtering of the along-track data. The sea surface height (SSH) built from *ocean* retracking (see Envisat RA2-MWR Handbook, 2007, http://envisat.esa.int/handbooks/ra2-mwr/) is corrected for path delay effects (wet and dry troposphere, ionosphere, etc.) (see *Le Traon and Ogor* [1998] and *Le Traon and Ogor* [2003] for details) and for geophysical effects. The tide model used is GOT00.2 (based on spectral analysis of tide gauge and altimetric signals) [*Ray*, 1998]. The barotropic response of the ocean to atmospheric pressure forcing and wind effects is modeled by a correction based on a combination of the classical inverse barometer (IB) correction for low frequencies (lower than 1/20 day^{-1}) and the Modèle aux Ondes de Gravité 2-dimensions (MOG2D) [*Carrère and Lyard*, 2003] for higher frequencies.

[13] The data are sampled every 350 m (for 20 Hz data) or resampled every 7 km (for 1 Hz data) along the tracks using cubic splines. A mean profile, <SSH>, is removed from the individual SSH measurements, yielding sea level anomaly (SLA) values. The mean profile contains the geoid signal

Table 2. Glider Cruise Characteristics: Dates, Total Length (Lineal and Real Distances) and Number of Profiles

	Go Date	Return Date	Total Cruise Lineal Distance (Go + Return, km)	Total Cruise Real Distance (Go + Return, km)	Mean Distance Between Profiles (km)	Total Profiles[a]
Jul 2007	06072007	13072007	176	188	0.71	269
Nov 2007	23112007	30112007	88	107	0.54	201
Apr 2008	07042008	23042008	318	388	0.30	1321
Jun 2008	20062008	24062008	84	97	0.29	335

[a]During the 2007 missions, only downcasts were collected, whereas for the missions in 2008, both downcasts and upcasts were collected.

and the mean dynamic topography over a 7 year averaging period (1993–1999).

[14] A key aspect of our data processing is the editing, that is to say, the method of selecting good altimetric data over corrupted data (see section 3.1.1). In official standard products, for example that of *Ruiz et al.* [2009b], the remaining measurement noise is reduced by applying Lanczos cutoff and median filters for a 42 km window to the 1 Hz SLA. That 42 km filter could, however, generate too much smoothing of the SLA, given the spatial scales associated with coastal dynamics (first Rossby radius of ~14 km in the Mediterranean Sea) [*Robinson et al.*, 2001]. Moreover, the small length of glider cruises associated with this window size could entail predominant edge effects along the whole track (see section 3.1.3).

2.1.2. Gridded Field Product

[15] Multisatellite AVISO (M)SLA are also used. The corrected along-track SSH obtained for each mission (Jason-1 and Envisat for the period analyzed in this study) have been inter-calibrated with a global crossover adjustment of the Envisat data using Jason-1 data as a reference [*Le Traon and Ogor*, 1998]. The mapping method to produce (M)SLA from along-track data is detailed in *Le Traon et al.* [2003] and consists of a suboptimal space-time objective analysis that takes into account along-track correlated errors. The products used in this study are specific for the Mediterranean Sea. For information on resolution, correlation scales, and measurement noise see *Pujol and Larnicol* [2005].

[16] For each set of SLA (1 Hz, 20 Hz, and (M)SLA), a mean dynamic topography (MDT) has been added in order to obtain the ADT. Here, we use a regional MDT of the Mediterranean Sea, as described by *Rio et al.* [2007], resulting from a combination of model outputs, drifting buoys, and altimeter data. This MDT was built to be compatible with altimetry, i.e., it represents a MDT averaged over the same period (1993–1999) as the temporal mean that is removed to compute SLA.

2.2. Data From Gliders

[17] We used data from repeated glider surveys in the Balearic Sea conducted between July 2007 and June 2008 (see Table 2 for details). Gliders are autonomous underwater vehicles providing high-resolution hydrographic and biogeochemical measurements. These vehicles control their buoyancy to allow vertical motion in the water column and make use of their hydrodynamic shape and small fins to induce horizontal motions. The platform used in this study is a Teledyne Webb Research Slocum Electric glider for shallow water (200 m maximum depth) with a net horizontal speed of ~25 km/d, which takes into account data transmission when the glider is at the surface, once every 6 hours in this type of survey.

[18] In all of the missions, the glider operated between surface and 180 m. During the first surveys in 2007, only downcasts were collected whereas for the missions in 2008 both downcasts and upcasts were registered, obtaining spatial resolutions of ~600 and ~300 m, respectively. However, as shown in Table 2, spatial resolution is not a constant value as it depends on how the glider is ballasted as well as on the presence of intense currents. Glider conductivity-temperature-depth (CTD) profiles were processed and calibrated against independent CTD casts from the SeaBird-19 probe installed on the Mediterranean Institute for Advanced Studies (IMEDEA) ship. Profiles extracted from glider data were corrected for thermal lag using the recursive filter introduced by *Lueck and Picklo* [1990] and *Morison et al.* [1994]. The final profiles were vertically averaged into 1 m bins.

[19] Surface geostrophic currents can be estimated from the glider surface DH (obtained from temperature and salinity fields) with respect to an arbitrary reference level which is in general considered to be at the maximum depth of the glider measurements (here 180 m). This implies that geostrophic velocities at this reference level are negligible, which is not always a correct assumption as many dynamical features usually have a deeper extension. However, depth averaged absolute currents can also be retrieved from GPS glider positioning, which gives one reference velocity vector for every ~7 km at every glider surfacing. The attitude sensor of the platform and the angle of attack can introduce an associated error in the cross- and along-track estimates of depth averaged currents of about 2–3 cm/s [*Merckelbach et al.*, 2008].

3. Absolute Sea Surface Geostrophic Current Computation

3.1. Absolute Surface Geostrophic Current From Altimetry

3.1.1. Editing Procedure and Impact on the Coastal Data Retrieval

[20] The use of high-frequency along-track sampling (20 Hz, ~350 m) allows small scale dynamics, as present in the northwestern Mediterranean, to be captured. However, this high-resolution altimetric data is extremely noisy and must be edited [see *Bouffard et al.*, 2008]. In this study, the determination of altimetric outliers is based on the assumption that deviations of measurements from the mean value should vary spatially smoothly and follow a uniform distribution. Outliers can be detected when the deviations exceed a pre-determined range in the ranked deviation series. We propose here to use three times the standard deviation (3σ) of along-track SLA as the upper and lower limits to remove main residual outliers related to land contaminations. This 3σ selection procedure is repeated 10 times (iterative process).

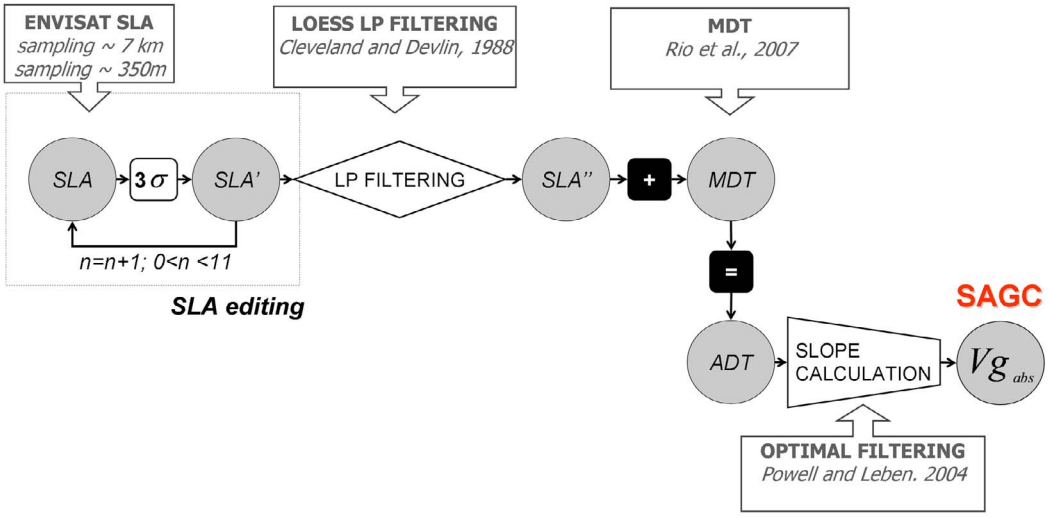

Figure 2. Altimetric surface absolute geostrophic current (SAGC) processing scheme.

The edited along-track SLA are then spatially low-pass (LP) filtered using a 20 km Loess filter [*Cleveland and Devlin*, 1988]. This quality control procedure is applied to the 20 Hz (or 1 Hz) fully corrected along-track data (see Figure 2).

[21] Our editing strategy has no impact on the 1 Hz data (data are pre-edited, for more details refer to section 4 of the Envisat RA2/MWR ocean data validation and cross-calibration activities, yearly report 2008, http://www.aviso.oceanobs.com/fileadmin/documents/calval/validation_report/EN/annual_report_en_2008.pdf). The data selection, however, impacts on the 20 Hz along-track altimetric SLA eliminating efficiently land-contaminated data from 2%–15% of the 20 Hz original data set, especially in the 20 km coastal band (see triangles in Figure 3, right).

[22] In general, in the 50 km coastal band, data close to the coast are more likely to be eliminated by the editing procedure because altimeter and on-board radiometer footprints may encounter land. Apart from November 2007, where only few data points are eliminated along the whole track (<2%), more than 25% (65% in July 2007) of the original data are excluded at 21–28 km distances from the coast (see Figure 3, left). Despite data eliminations by our editing procedure, Table 3 shows that the 20 Hz sampling allows us to recover more data than the 1 Hz data in close proximity to the coast; between 6 and 13 km closer to the coast by recovering 10 points measurements between the last 1 Hz available data and the coastline and by applying the 3 σ statistical criterion to more data (20 times more than at 1 Hz).

3.1.2. From Sea Level Anomaly to Surface Absolute Geostrophic Current

[23] The across-track SAGC is calculated by adding the interpolated MDT to the edited and filtered SLA (see section 3.1.1 and Figure 2). By construction, this current is perpendicular to the satellite track, so in our case it is almost parallel to the Balearic and Iberic shelf break (see Figure 1) which should allow us to intercept the main components of dynamics related to BC and NC.

[24] The across-track altimetric SAGC is given by

$$Vg_{\mathrm{abs}} = \frac{g}{f}\frac{\partial(\mathrm{SLA}' + \mathrm{MDT})}{\partial x}, \qquad (1)$$

where g is the gravitational acceleration, f is the Coriolis parameter, x is the axis set along the track direction, SLA′ is the residual filtered sea level anomaly (from both edited 1 and 20 Hz data) and MDT is the mean dynamic topography [from *Rio et al.*, 2007].

[25] The along-track altimetric gradient is estimated by using the optimal filter developed by *Powell and Leben* [2004] with a spatial frame of 20 km. In the next sections, even if not precise, the computed altimetric SAGC corresponds to components that are perpendicular to Envisat track 773.

3.1.3. Sensitivity to Altimetric Noise

[26] Very few studies have analyzed the noise content of 20 Hz altimetric SLA. Recent comparisons between 20 Hz altimetric SLA and tide gauges in the western Mediterranean Sea indicate that 20 Hz altimeter measurement errors range from 2 to 5 cm, mainly depending on the data editing and smoothing process [*Bouffard et al.*, 2008, 2010].

[27] Here, a Monte Carlo procedure is employed in order to test the sensitivity of the SAGC computations to any remaining noise in the 20 Hz edited SLA. To perform the Monte Carlo simulation, an artificial data set was created by adding Gaussian random noise with zero mean to the original SLA. Here, for 20 Hz altimetric signals (before the spatial filtering), the spatial standard deviation (STD) noise level is set at 5 cm (which approximately corresponds to the spatial STD of the edited 20 Hz SLA for the missions used). The resulting corrupted SLA was used to generate new estimates of the SAGC following the methodology described in Figure 2. A total of 10,000 Monte Carlo simulations were carried out for each of the four missions.

[28] For the missions of July 2007, November 2007, April 2008, and June 2008 the spatial mean of the STD difference

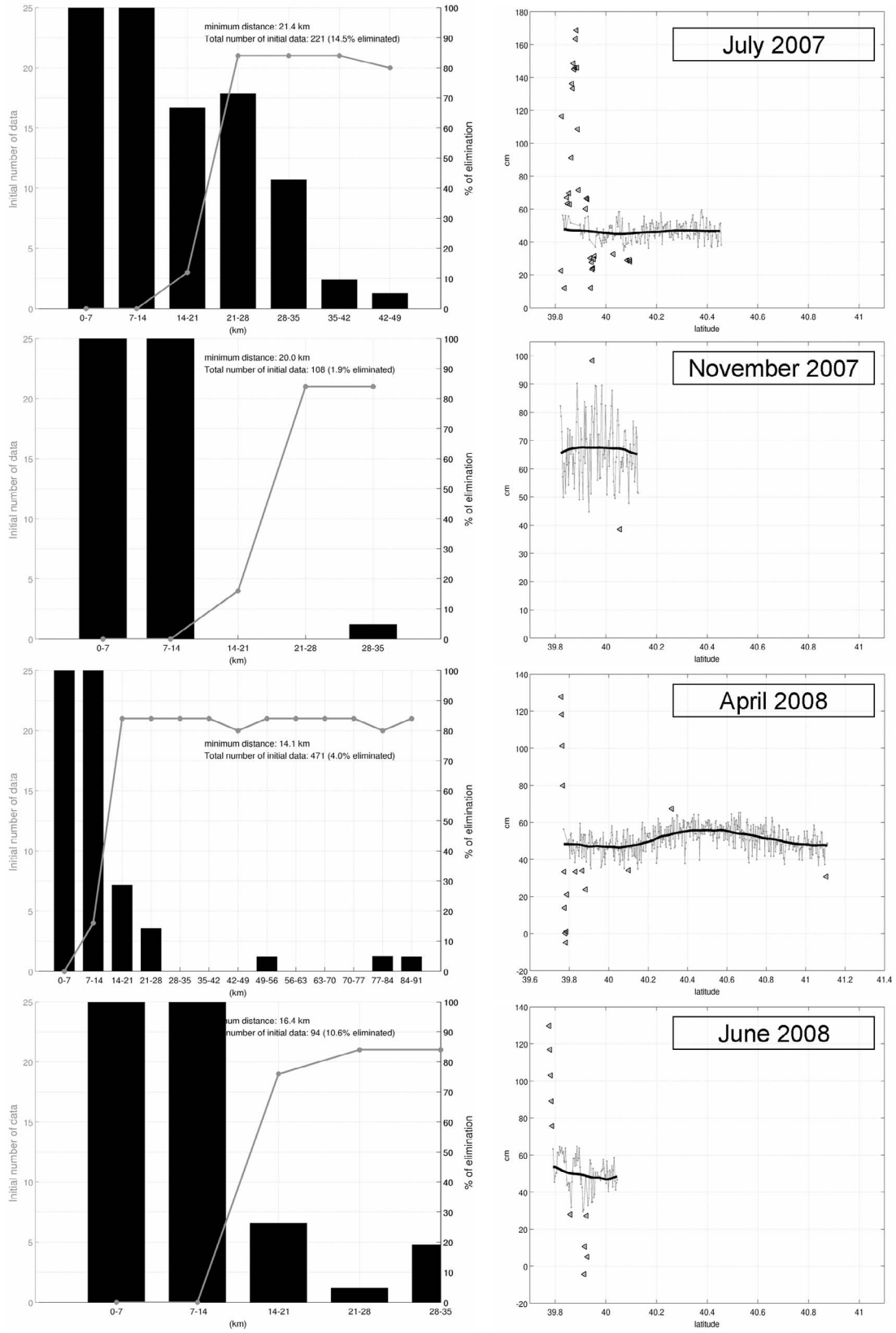

Figure 3. (left) Percentage of raw 20 Hz altimetric data eliminated (black histograms) and number of original data (shaded curve) as functions of distance to the coast (by 7 km class). (right) Sea level anomaly (SLA; 20 Hz, cm) as a function of latitude (°N) and corresponding impact of editing. Triangle, eliminated SLA; shaded curve, edited SLA; black curve, edited and 20 km low-pass (LP)-filtered SLA.

Table 3. Distance From the Coast to the Closest Valid Altimetric Measurements for Each Mission[a]

	Jul 2007	Nov 2007	Apr 2008	Jun 2008
1 Hz	34.2	27.2	20.3	26.8
20 Hz	20.6	20.0	12.8	14.7
20 Hz + editing	21.4	20.0	14.1	16.4

[a]Distances in km.

between signals a and b (STD(a-b)) between uncorrupted and corrupted SAGC are 6.3, 9.5, 4.7, and 8.5 cm/s, respectively, while the mean differences are close to 0 cm/s along the whole transect (see Figure 4, shaded curve). This means that the SLA noise impacts the SAGC gradient but not its spatial average. The differences of mean STD errors as a function of missions are mainly due to the length of track used (see Table 2) and the relative weight of edge effects used to determine the averaged errors along the whole track. Thus, the longer the mission, the lower the averaged STD error. Figure 4 shows an example of the Monte Carlo simulation for the mission of April 2008.

[29] As shown in Figure 4 (black curve), outside of the 20 km edge of the track (i.e., the window used both for the LP Loess filtering and slope calculations), the Monte Carlo STD are less than 5 cm/s whereas in the first and last 20 km of the track, the associated errors increase and become higher than 10 cm/s because of edge effects. This suggests that only missions of sufficient length (i.e., >40 km as in the July 2007 and April 2008 missions) can be used to efficiently assess the gradient of across-track SAGC with respect to the geostrophic velocities computed from glider. The other missions, November 2007 and June 2008, have too short a length for gradient SAGC comparisons; however, they can be used to assess the mean SAGC.

[30] In summary, when we look at the whole mission, the averaged error due to the altimetric noise is about 0 cm/s along the whole track, whereas the associated STD errors are between 4 cm/s (>20 km from the coast) and 10 cm/s (within 20 km of coast). These error values are of the same order of magnitude as the STD differences that *Vignudelli et al.* [2005] (respectively, *Bouffard et al.* [2008]) found by performing a direct comparison in the Corsica Channel between improved along-track TOPEX/Poseidon-derived (respectively, improved multisatellite-derived) velocities and mooring velocity anomalies.

3.1.4. Impact of Sampling and Editing on the Velocity Computation

[31] As shown previously, the geostrophic slope calculation is sensitive to the SLA noise, especially in the coastal zone. This indicates the crucial importance of SLA editing before SAGC computation. Figure 5 clearly shows the impact of this editing on altimetric velocities for the missions of July 2007 and April 2008.

[32] From Figure 5 it appears that the SLA editing has a strong influence on the SAGC computation, especially within a 50 km coastal zone (Figure 5, dashed boxes). Indeed when the editing procedure is not applied, the resulting coastal SAGC values are unrealistically large in July 2007 (>80 cm/s). In April 2008, the editing also entails deep modifications in the coastal area where the SAGC values derived from edited SLA are about 15 cm/s. Beyond a 50 km coastal band, the editing has less influence as less data are eliminated (see section 3.1.1).

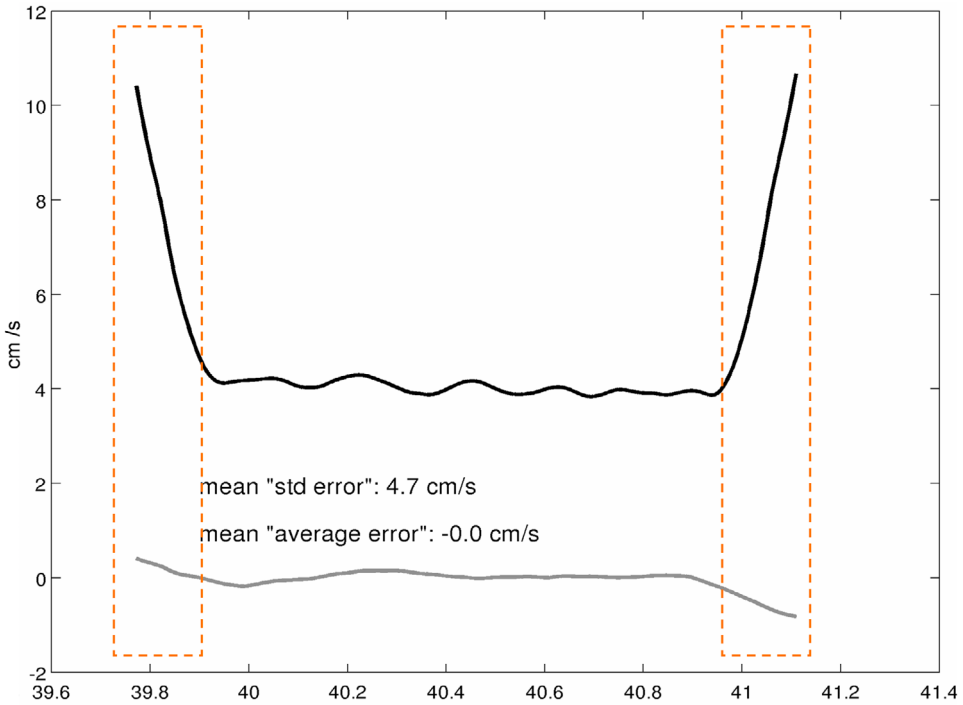

Figure 4. Errors (cm/s) obtained from Monte Carlo simulation as a function of latitude (°N), for the mission of April 2008. Shaded curve, average error; black curve, standard deviation (STD) error. The dashed orange rectangles indicate areas where the STD error is greater.

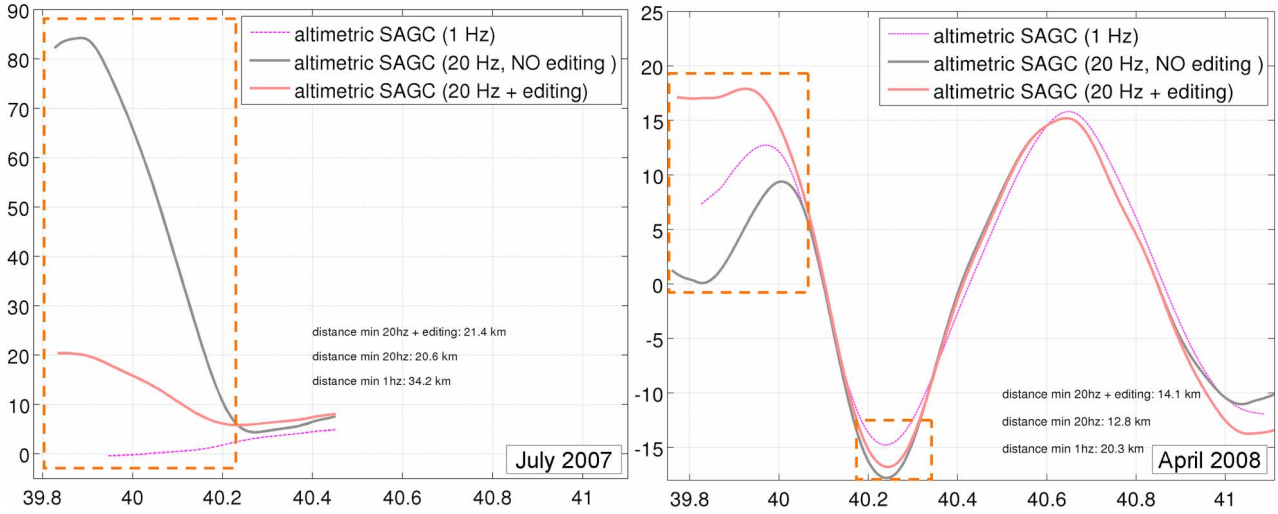

Figure 5. Altimetric across-track surface absolute geostrophic current (SAGC; cm/s) as a function of latitude (°N) derived from 1 Hz (pink thin curve), raw 20 Hz (shaded thick curve), and edited 20 Hz SLA (red thick curve) in (left) July 2007 and (right) April 2008. Areas with major differences are located inside the orange dashed boxes.

[33] When comparing with velocities computed from 1 Hz SLA, significant differences are also observed. In July 2007, the 1 Hz SAGC are very low in the 50 km coastal zone whereas a relative strong current (between 10 and 20 cm/s) is observed by using the 20 Hz edited data. In April 2008, differences are also observed in the neighborhood of the BC where the 1 Hz SAGC exhibits a current 5 cm/s less than that from edited 20 Hz data. This is also the case between 40.1°N and 40.4°N.

[34] In section 3.2, a direct comparison with glider calculated velocities provides robust insights about the respective performance of these different along-track altimetric data sets.

3.2. Absolute Surface Geostrophic Velocity From Glider Data

3.2.1. General Methodology and Reference Level Issue

[35] *Ruiz et al.* [2009b] used a reference depth level of 180 m to estimate $DH_{z_{180}}$ from glider data and obtained coherent glider geostrophic velocities flowing northeastward along the north Mallorca coast. For specific events, velocity estimates from 42 km smoothed $DH_{z_{180}}$ appeared to be not very sensitive to the test reference level, seeming to indicate that the layer between 200 and the bottom does not play a key role in the dynamics of the upper layer. However, on closer consideration, small differences in $DH_{z_{180}}$ gradients entail significant modifications in the geostrophic velocity pattern and magnitude. For this reason, a more robust strategy has been developed in this study. This strategy aims at solving the reference level issue by combining glider CTD current ($Vg_{z_{180}}$: cross-track geostrophic component of the baroclinic current relative to 180 m), glider GPS current ($\overline{V_{\mathrm{abs}}}$: 180 m depth average absolute current), and model outputs. Figure 6 shows the scheme used to process glider SAGC.

[36] At each vertical level z, $Vg_{z_{180}}$ is derived from the $DH_{z_{180}}$ using an optimal filter as described by *Powell and Leben* [2004] (as used in the altimetry data). Then, the difference between the 180 m depth average $\overline{Vg_{z_{180}}}$ and $\overline{V_{\mathrm{abs}}}$ should correspond to the absolute velocity at 180 m. By adding a reference level correction (RLC, $\overline{V_{\mathrm{abs}}} - \overline{Vg_{z_{180}}}$) to $Vg_{z\,=\,0_{180}}$ at the surface, we should therefore be able to compute the glider SAGC.

[37] However, these two averaged velocities do not have exactly the same physical content. Whereas $\overline{V_{\mathrm{abs}}}$ is influenced by the whole depth averaged dynamical components, including ageostrophy, high-frequency barotropic signals, cyclostrophy, and inertial current, $\overline{Vg_{z_{180}}}$ is only the result of the baroclinic geostrophy contribution. Therefore, $\overline{V_{\mathrm{abs}}}$ needs to be partially corrected by using modeled high frequency geophysical corrections (HFGC, MOG2D + Ekman currents).

3.2.2. High-Frequency Geophysical Corrections (HFGC)

3.2.2.1. Ageostrophic Ekman Effects

[38] The Ekman current is the motion induced by the wind according to the theory of *Ekman* [1905] and should represent one of the main ageostrophic contributions included in $\overline{V_{\mathrm{abs}}}$ but which is missing in $Vg_{z_{180}}$. In this study, an Ekman component has been estimated following the method of *Poulain et al.* [2009]. The wind data used are from SeaWinds on QuikSCAT Level 2B Ocean Wind Vectors in 25 km Swath Grid (http://cersat.ifremer.fr/fr/data/discovery/by_parameter/ocean_wind/quikscat_l2b). To remove the very high frequency signals, which have no impact on the Ekman oceanic motion, the data have been filtered with a low-pass filter at a 36 hours cutoff frequency. Given that the angle ϕ between the wind and surface motion (in theory $\pi/4$) and Ekman depth D strongly depend on location and time [*Rio and Hernandez*, 2003], we therefore evaluate those parameters by using three drifters launched over the Balearic Sea. We found values of $\phi = 24°$ and averaged depth $D = 36$ m, which are in agreement with past studies of the Mediterranean Sea [see *Ursella et al.*, 2006; *Poulain et al.*, 2009]. The Ekman current was then validated with independent drifter velocities [*Escudier*, 2009], 180 m depth averaged (assuming

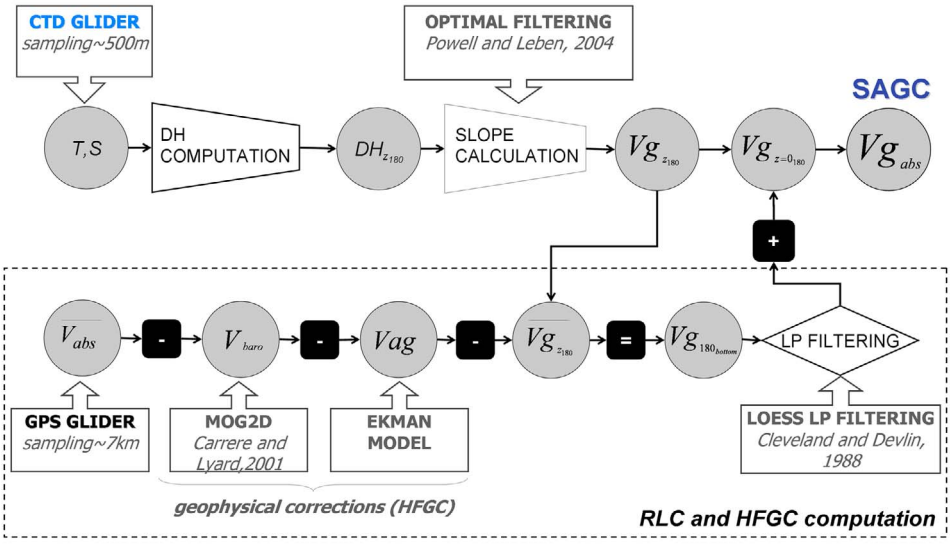

Figure 6. Glider surface absolute geostrophic current (SAGC) processing scheme.

the theoretical spiral in the Ekman layer and approximating to 0 cm/s below), space-time interpolated at glider positions, and removed from $\overline{V_{\mathrm{abs}}}$.

3.2.2.2. Barotropic High-Frequency Current

[39] Barotropic currents induced by high-frequency atmospheric forcing are not included in $Vg_{z_{180}}$ and, in theory, have also to be removed from $\overline{V_{\mathrm{abs}}}$ (see Figure 6). For this, we use a correction of the ocean response to atmospheric wind and pressure forcing from the MOG2D finite element barotropic model [*Carrère and Lyard*, 2003] for high frequencies (i.e., <20 days), and an IB correction for lower frequencies. The model is forced by surface atmospheric pressure and wind from European Centre for Medium-Range Weather Forecasts analysis. Barotropic currents are provided on a regular grid of 0.25° × 0.25° every 6 hours and space-time interpolated at glider positions.

4. Dynamical Structures Observed

4.1. Surface Patterns and Associated Vertical Structures

[40] In this section, surface patterns (from remote sensing) are qualitatively compared to the vertical structures (from glider). We use both $\overline{V_{\mathrm{abs}}}$, sea surface temperature (SST), SAGC derived from (M)SLA, and glider baroclinic geostrophic velocities derived from single CTD measurements ($Vg_{z_{180}}$) projected onto the Envisat-altimetric track 773 position. Figure 7 shows an example of the combined use of remote sensing and a glider when observing dynamics in our study area during the "go" glider transect (northward). For the missions of July 2007, November 2007, and June 2008 (respectively, April 2008), the glider cruise began approximately 3 days (respectively, 7 days) before the Envisat passage and crossed several dynamical patterns where significant across-track surface currents were observed (see Figure 7).

[41] In July 2007, the glider intercepts the BC in the coastal Balearic zone (Figure 7a). Farther north, the remote sensed SST data shows a marked thermal front corresponding to the Catalan front and an associated south border of the NC is seen. In addition, between these two major dynamical patterns an eddy is also observed in the velocities. The southwestern branch of this eddy is almost parallel to the glider position which means that the associated across-track velocity would not be clearly seen by the glider. This is confirmed when we look at the glider transect where, out of the BC, the across-track velocity is low. It also appears that the BC, which borders the coast of Mallorca, is enlarged by about 40 km large and marked by a significant velocity in the first 50 m depth (double that at 100 m).

[42] Figure 7b shows that the general situation in November 2007 is close to the one observed in July 2007. The SST also shows a marked Catalan front in the north associated with the NC cooling. In the south, the BC is further away from the coast (about 10 km). A current loop, which extends at 60 km from the Mallorca coast, is clearly observed in both SST and SAGC velocity. This loop joins the western branch of an eddy based north of the BC. Unfortunately, the length of the glider cruise does not allow us to capture the vertical structure of this eddy. When we look at the glider transect it can be seen that the BC surface intensity is approximately double that of July 2007, moreover the current has a deeper expression extending to ~100 m. The computed velocities from remote sensing, indicate that the BC flows at distance higher than 10 km to the Mallorca coast whereas it was close along the coast in July 2007, which is also confirmed by $\overline{V_{\mathrm{abs}}}$.

[43] In April 2008, the general circulation characteristics are quite different (compare Figure 7c). The SST image shows a marked Balearic front whereas the Catalan front is much weaker. Moreover, the glider cruise intercepts three major dynamical structures: the BC in the south, the NC in the north, and an eddy in between. The across-track velocities associated with these features appear clearly both at surface and along the whole 180 m water column in the glider CTD and GPS measurements. The velocities associ-

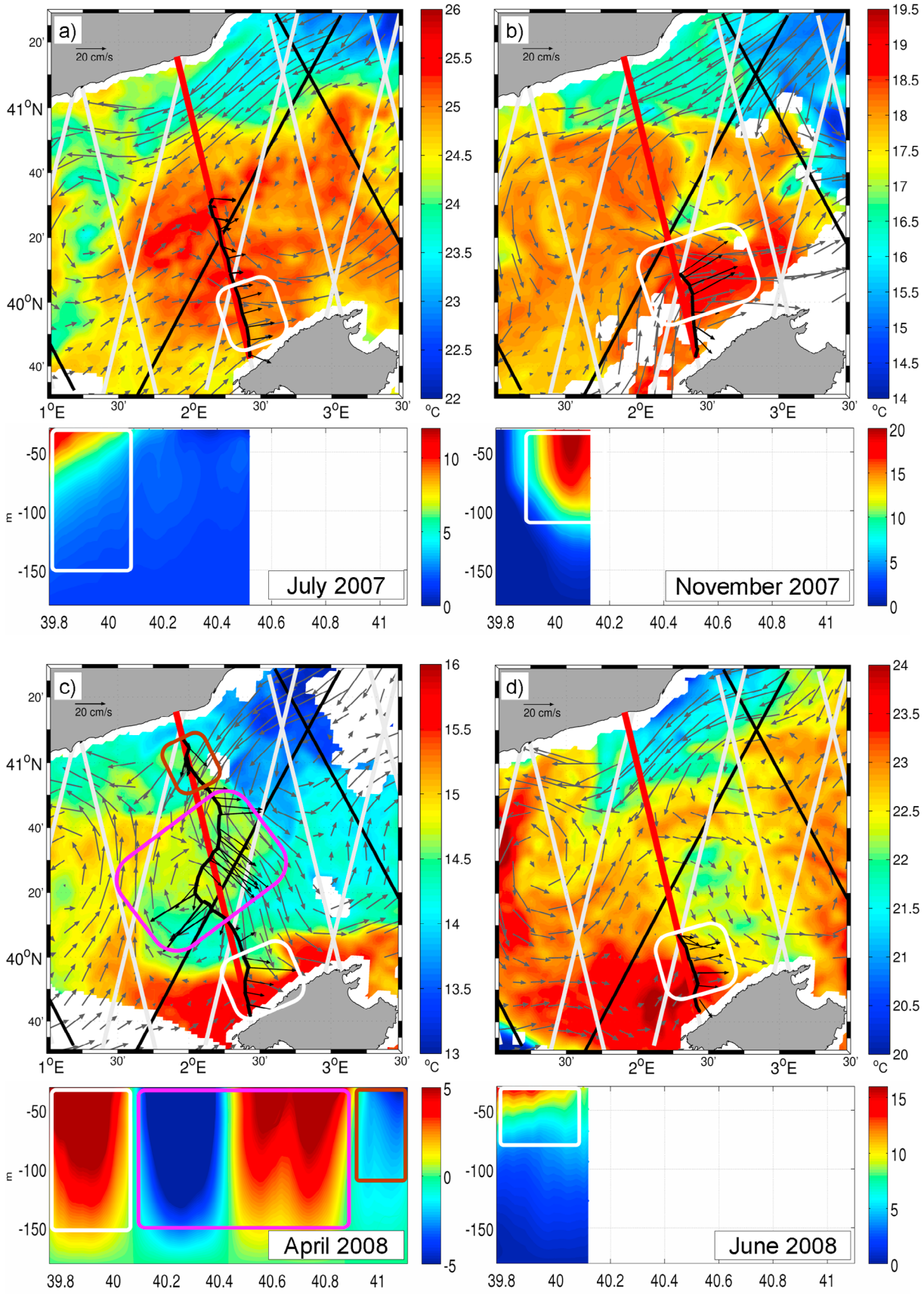
a)
b)
c)
d)
20 cm/s
41°N
40°N
1°E
2°E
3°E
°C
m
July 2007
November 2007
April 2008
June 2008
39.8
40
40.2
40.4
40.6
40.8
41

Figure 7

Table 4. Mean and Standard Deviation of Glider GPS ($\overline{V_{\text{abs}}}$) and Conductivity-Temperature-Depth (CTD, $Vg_{z_{180}}$) Currents for Both Go and Return Cruises[a]

	Jul 2007 $\overline{\Delta t}$ = 6.8 d			Nov 2007 $\overline{\Delta t}$ = 2.6 d			Apr 2008 $\overline{\Delta t}$ = 14.4 d			Jun 2008 $\overline{\Delta t}$ = 2.4 d		
	Go	Return	Diff.[b]	Go	Return	Diff.[b]	Go	Return	Diff.[b]	Go	Return	Diff.[b]
						CTD						
Mean	4.4	4.0	0.4	11.5	−9.8	21.3	1.2	2.6	−1.4	13.8	11.8	2.0
STD	4.7	8.0	3.5	7.8	10.4	9.0	7.1	7.8	3.7	24.4	11.3	28.0
						GPS						
Mean	12.2	17.7	−5.5	19.6	20.2	−0.7	4.7	7.5	−2.8	16.5	24.5	−8
STD	2.5	4.5	2.1	7.1	9.5	3.0	13.1	13.4	8.8	2.0	1.1	0.9

[a]In cm/s.
[b]Diff. column corresponds to the difference between the "go" and "return" cruises. Given their short length in relation to the spatial filtering used (20 km), only the means are significant for the November 2007 and June 2008 missions, both of which are affected by the windows edge.

ated with the eddy are quite strong, being of the same order of magnitude as the BC ($Vg_{0<z_{180}<100} > 5$ cm/s). In the north, within the 20 km Iberian coastal band, the NC signature is also well identified showing a velocity with an opposite direction and less amplitude than in the BC.

[44] In June 2008, remote sensing shows (Figure 7d) that the situation is close to the one observed in July and November 2007 with a marked Catalan front at north. Between BC and NC, eddies are observed both east and west of the glider track. Even though the glider cruise is relatively short (42 km), the BC is captured. The transect shows a progressive decrease of BC intensity in the coast–open ocean direction, which is in agreement with the altimetric observations. It follows from altimetry that this decrease is probably due to the geometrical orientation of currents. Indeed, far away from the coast, the currents are again almost parallel with the glider position, thus the across-track component cannot be well captured.

[45] Those comparisons show good qualitative agreement and potential complementarily information arising from remote sensing and glider measurements. However, even if $Vg_{z_{180}}$ and the altimetric SAGC seem to be of same order of magnitude, we believe that they are both here underestimated (see stronger and almost colocalized $\overline{V_{\text{abs}}}$ in Figure 7). In addition to the synopticity issues, this specific point will be discussed in the next section through direct comparisons between $Vg_{z_{180}}$ at surface (from CTD glider), altimetric SAGC (from (M)SLA interpolate at the glider location) and $\overline{V_{\text{abs}}}$ (from GPS glider positioning).

4.2. Variability at Glider Mission Temporal Scale and Synopticity Issues

[46] Whereas along-track altimetry allows an instantaneous measurement (every 35 days for Envisat), glider cruises take several days (see Table 2) to complete a "go" transect (northward: Mallorca–Iberian coast direction) and "return" transect (southward: Iberian coast–Mallorca direction). This raises the crucial issue of temporal lags between the glider and altimetric measurement. In this respect, direct comparisons between go and return measurements of glider are used here to provide a first assessment of the time delay impact. Table 4 synthesizes the statistical characteristics, differences of go and return velocities and the associated mean time delay for the four glider missions.

[47] Table 4 shows that, the mean differences of $Vg_{z=0_{180}}$ (glider CTD current) between the go and return trips range from 0.4 to 23 cm/s. Apart from the mission of November 2007, the mean differences are less than 2 cm/s. The mission of November 2007 is short (44 km), so a strong and quick modification of BC at surface or in its baroclinic structure would largely affect averages and explains the difference between go and return (~21.3 cm/s). For the mission of July 2007, the STD difference of $Vg_{z=0_{180}}$ is 3.5 cm/s which is equivalent to the one obtained in April 2008. For the whole missions the mean and STD differences of $\overline{V_{\text{abs}}}$ (glider GPS current), between go and return transects, are relatively small compared to the initial values.

[48] Figure 8 is an illustration complementing Table 4 and showing the spatial variations between go and return velocities from both altimetric (M)SLA (SAGC), GPS ($\overline{V_{\text{abs}}}$), and CTD measurements ($Vg_{z=0_{180}}$) in July 2007 and April 2008.

[49] Figure 8 indicates that even if the same kind of dynamical patterns are observed, there are some major differences. In July 2007, $Vg_{z=0_{180}}$ (Figure 8a, left) shows equivalent magnitudes at go and return times whereas $\overline{V_{\text{abs}}}$ (Figure 8b, left) decrease at return time over the whole transect. In April 2008, even if the BC and eddy signatures are observed both at go and return time, significant differences appear (Figures 8a and 8b, right). This seems to be due to the eddy displacement and also to modifications in the intensity, depth, and position of the BC. It is therefore important to keep in mind that subsampled processes occurring at the glider mission temporal scale (<3 weeks) could

Figure 7. Surface circulation from remote sensing and the associated vertical structures from glider "go" (northward) missions of (a) July 2007, (b) November 2007, (c) April 2008, and (d) June 2008. Top images in Figures 7a–7d show SAGC in cm/s (shaded arrow) derived from map of sea level anomalies ((M)SLA) overlapped by snapshot sea surface temperature (SST, °C) and satellite altimetric tracks (black, Jason-1; white, Envisat; the Envisat track 773 is highlighted in red). Glider displacement (black curve) with corresponding GPS raw current ($\overline{V_{\text{abs}}}$, black arrows). Bottom images in Figures 7a–7d show projected across-track glider CTD velocity ($Vg_{z_{180}}$, cm/s) as a function of latitude (°N) and depth (in m). For both top and bottom images in Figures 7a–7d the areas inside the white squares indicate the Balearic Current (BC), pink squares indicate anticyclonic eddies, and brown squares the Northern Current.

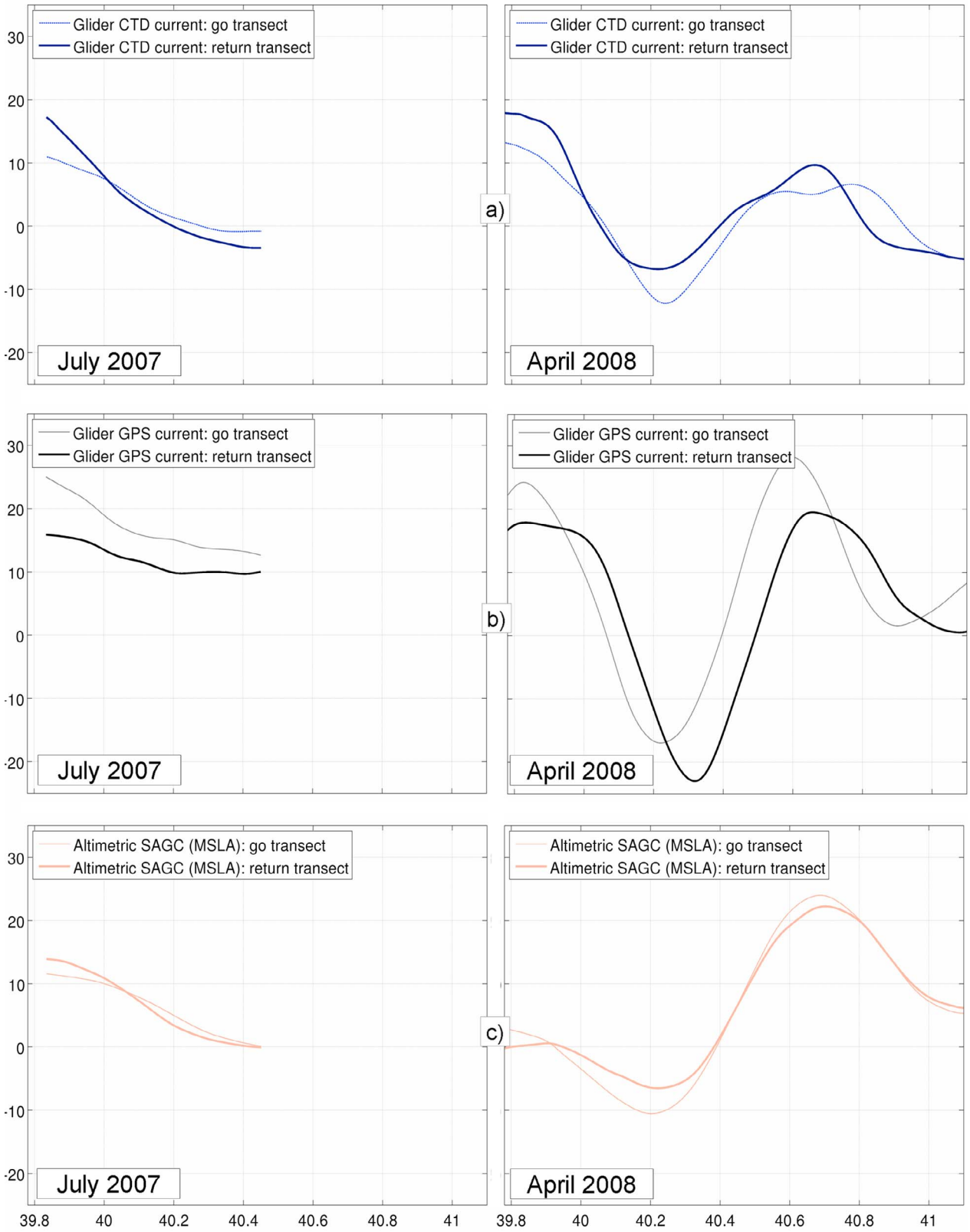

Figure 8. LP-filtered 20 km across-track currents (cm/s) interpolated at the Envisat track location in (left) July 2007 and (right) April 2008 as a function of latitude (°N) for both for "go" (thin curves) and "return" (southward; thick curves) missions: (a) surface glider CTD current ($Vg_{z=0_{180}}$, blue curves), (b) glider GPS current ($\overline{V_{\mathrm{abs}}}$, black curves), (c) altimetric across-track SAGC derived from (M)SLA (brown curve), with time interpolated at glider passage.

potentially affect the comparison between glider and along-track altimetry in section 5. They can also be the consequence of inexact colocalization between the two passages. In addition to high-frequency 3D processes, the differences could also have several causes that are difficult to distinguish such as error in glider measurements, especially concerning positioning at surface during data transmission or from attitude sensors providing glider heading, pitch and roll (see *Merckelbach et al.* [2008] for technical details). For the altimetric SAGC derived from (M)SLA (Figure 8c) no significant differences are observed between go and return missions, certainly because of the temporal smoothing effect due to the optimal interpolation (OI; 7 day windows) procedure.

[50] The altimetric SAGC from (M)SLA show a satisfactory agreement with $Vg_{z=0_{180}}$ and $\overline{V_{\text{abs}}}$ for the July 2007 and April 2008 missions except in the 40 km coastal band where the altimetric SAGC shows weaker gradients and amplitudes. Moreover, the magnitude of $\overline{V_{\text{abs}}}$ appear to be significantly stronger (>30%) compared to both $Vg_{z=0_{180}}$ and altimetric SAGC. There are several hypotheses that can explain these discrepancies; they will be discussed in the next section through the assessment of our new glider and altimetry SAGC processing. In addition to physical content nonhomogeneity and errors related to $\overline{V_{\text{abs}}}$, differences observed between $Vg_{z=0_{180}}$ and $\overline{V_{\text{abs}}}$ could result from a reference level issue (issue specifically addressed in section 5.1.1). Concerning the observed underestimation of altimetry SAGC toward $\overline{V_{\text{abs}}}$, it could be partially due to spatial smoothing. Indeed, (M)SLA has been smoothed through an OI procedure which uses a correlation length scale of 100 km. Moreover, before OI, the altimetric along-track data (refer to the track positions in Figure 7) has been low-pass filtered with a cutoff of 42 km. This is why, in the next sections, we will compute altimetric SAGC directly from along-track data following the methodologies described in section 3.1. Impact of the MDT, spatial filtering, sampling, and editing will be evaluated by direct comparisons with glider SAGC.

5. Cross-Validation of Along-Track Altimetry and Glider Velocities

5.1. Assessment of the Glider Velocity Processing

5.1.1. Impact of the Reference Level Correction

[51] Figure 9 shows comparisons between altimetric (built from 20 and 1 Hz edited along-track data) and temporal interpolated glider SAGC (using go and return transects) for the missions of July 2007 and April 2008 with and without the application of RLC (impact of HFGC is very small here and thus will be discussed independently in section 5.1.2).

[52] From Figures 9a and 9b it follows that there is a very good coherency between glider and altimetric velocities, coherency that is better than the observed with (M)SLA in the previous section. The signals are very well phased both with and without the application of RLC.

[53] In July 2007, a progressive decrease of velocity is seen in the Mallorca coast–open ocean direction. Between 40.0° and 40.2°N (i.e., inside the BC current), the glider and altimetry curves show a very similar slope. After 40.2°N, the velocity increases slightly in altimetry data whereas this is not the case with glider data. In April 2008, the BC is well identified. This current is associated with a relatively strong velocity (>15 cm/s) which progressively decreases moving offshore from the Mallorca coast. The anticyclonic eddy is observed in the two data sets; this dynamical structure, which crosses the Envisat track, is centered at about 40.5°N in latitude and its associated velocity is between −20 and 20 cm/s (see Figures 9a and 9b).

[54] Even if glider and altimetric velocity show a good agreement, significant differences are observed if RLC is not applied. In July 2007, the altimetric SAGC is stronger than $Vg_{z=0_{180}}$ (by 7.5 cm/s on average, see Figure 9a); however, the application of the RLC increases the mean glider velocity and therefore improves the agreement with altimetry (mean difference of 3.5 cm/s, see Figure 9b). Moreover, the percentage of STD explained by glider in altimetry becomes 75% with RLC application against 68% without RLC. In April 2008, the use of the RLC also improves significantly the agreement between glider and altimetry by increasing the glider velocity magnitudes (STD of 6.9 cm/s without RLC against 14.9 cm/s with). The percentage of STD explained by glider SAGC in altimetric SAGC is thus again improved (47% with RLC against 6% without).

[55] For missions of November 2007 and June 2008 the length of missions are too short for statistical comparisons of STD (see section 3.1.3). However, we can look at the mean SAGC inside the BC. For June 2008, the RLC also allows significant increases in the agreement between glider and altimetric SAGC with a mean difference of 17.4 cm/s without RLC against 0.7 cm/s with RLC (for a mean current of ~30 cm/s). In November 2007, $Vg_{z=0_{180}}$ shows a mean velocity of 5 cm/s. If the RLC is added, the glider SAGC becomes 25.5 cm/s, which is 13.9 cm/s more than for altimetry. This difference could be due to high-frequency dynamics not captured at the time of altimetric satellite passage. Indeed the mean difference between the go and return glider cruise is large for this mission (see Table 4) which support this suggestion.

[56] To sum up, the application of RLC enables the general improvement of the agreement between the glider and altimetry currents. However, it is important to note that for the whole mission the glider SAGC magnitudes are stronger than the altimetric ones. In addition to the combined effects of different errors (such as residual coastal altimetry contamination, inaccuracy of the MDT, and compass error for gliders), the underestimation observed in altimetry could be partially due to its inexact colocalization with the glider that can be influenced and partially advected by the strong currents (see differences between lineal and total glider cruise distances in Table 2). In April 2008, such differences are particularly observed at the eddy location. There, the altimetric SAGC underestimation could also come from the cyclostrophic acceleration, neglected in the geostrophic framework computation. This component, in the case of an anticyclonic eddy with the characteristics of the one studied here could be around 10%–20% of the geostrophic part of the velocity [*Gomis et al.*, 2001].

5.1.2. Impact of the High-Frequency Geophysical Correction

[57] The HFGC consists of the Ekman and MOG2D velocities which have been interpolated spatially and temporally along the glider position measurements. Table 5 summarizes their statistical characteristics for the missions

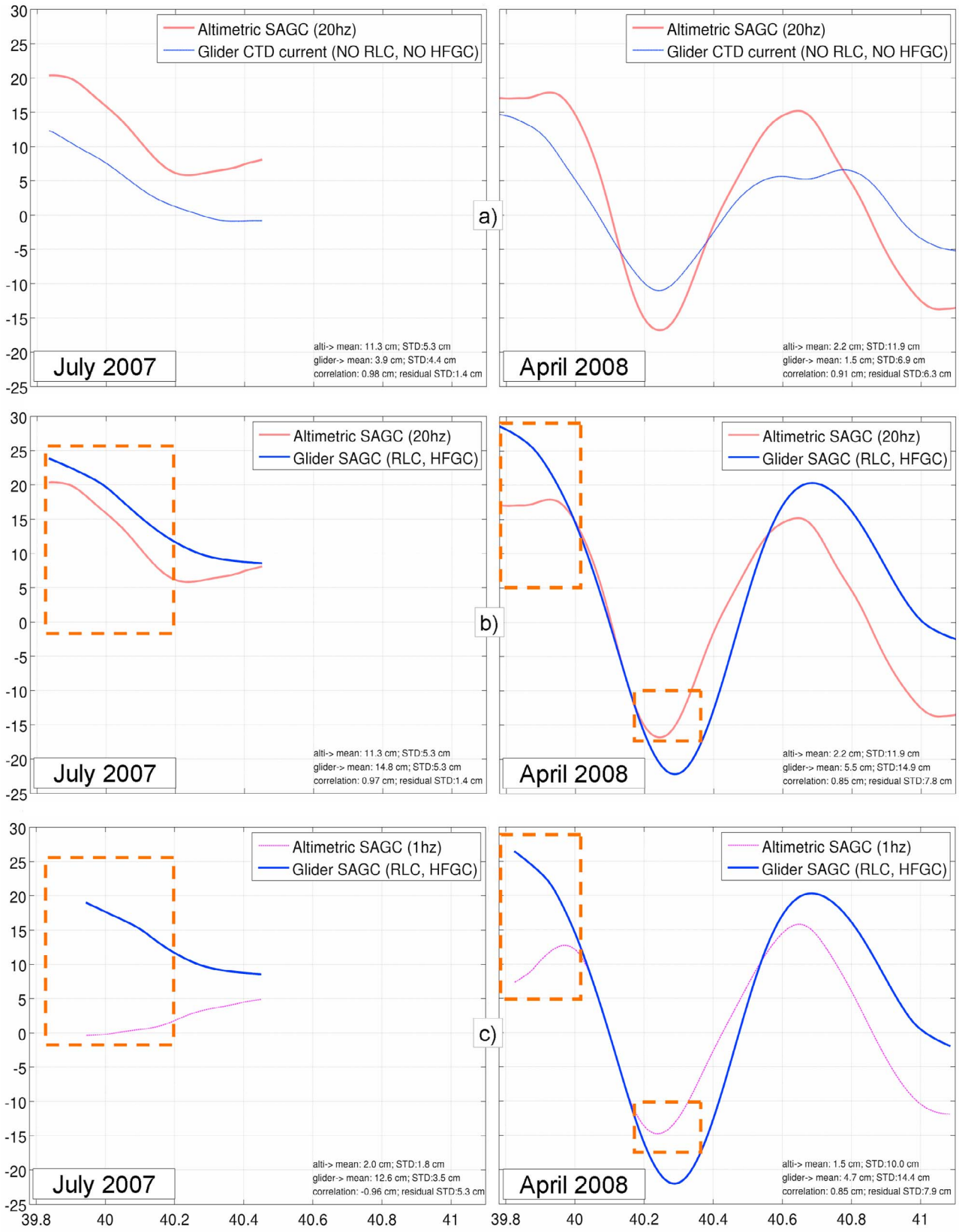
Altimetric SAGC (20hz)
Glider CTD current (NO RLC, NO HFGC)
July 2007
alti-> mean: 11.3 cm; STD:5.3 cm
glider-> mean: 3.9 cm; STD:4.4 cm
correlation: 0.98 cm; residual STD:1.4 cm
April 2008
alti-> mean: 2.2 cm; STD:11.9 cm
glider-> mean: 1.5 cm; STD:6.9 cm
correlation: 0.91 cm; residual STD:6.3 cm
a)
Altimetric SAGC (20hz)
Glider SAGC (RLC, HFGC)
July 2007
alti-> mean: 11.3 cm; STD:5.3 cm
glider-> mean: 14.8 cm; STD:5.3 cm
correlation: 0.97 cm; residual STD:1.4 cm
April 2008
alti-> mean: 2.2 cm; STD:11.9 cm
glider-> mean: 5.5 cm; STD:14.9 cm
correlation: 0.85 cm; residual STD:7.8 cm
b)
Altimetric SAGC (1hz)
Glider SAGC (RLC, HFGC)
July 2007
alti-> mean: 2.0 cm; STD:1.8 cm
glider-> mean: 12.6 cm; STD:3.5 cm
correlation: -0.96 cm; residual STD:5.3 cm
April 2008
alti-> mean: 1.5 cm; STD:10.0 cm
glider-> mean: 4.7 cm; STD:14.4 cm
correlation: 0.85 cm; residual STD:7.9 cm
c)
30
25
20
15
10
5
0
-5
-10
-15
-20
-25
39.8
40
40.2
40.4
40.6
40.8
41

Figure 9

Table 5. Ekman and Barotrophic Current Statistical Characteristics Interpolated (in Space and Time) at Go and Return Glider Positions[a]

	Jul 2007		Apr 2008	
	Go	Return	Go	Return
		Ekman		
Mean	0.3	0.1	0.5	0.2
STD	0.1	0.0	0.2	0.2
		MOG2D		
Mean	0.1	0.1	0.1	0.2
STD	0.1	0.1	0.2	0.0

[a]In cm/s.

of July 2007 and April 2008 and highlights that both Ekman and barotropic high-frequency velocities are very small (subcentimetric) for the considered period.

[58] The impact of HFGC is therefore marginal, especially compared to the RLC (small for Ekman and negligible for MOG2D). Moreover, the Ekman and MOG2D velocities are less than the amplitude of errors associated with both glider and altimetric velocity computations (problem of spatial synopticity, noise, etc.). In this respect, even if the use of HFGC is theoretically justified, the present comparison between glider and altimetry does not allow us to evaluate quantitatively its impact. However, the small reduction of the glider and altimetric SAGC mean differences for all missions (between 0.3 and 0.6 cm/s) gives few positive insights.

5.2. Assessment of the Coastal Altimetric Velocity Processing

[59] In the coastal zone, altimetric velocities are particularly affected by noise measurements (see section 3.1.3) while this is less the case for glider velocities. In this regard, the glider velocities are now used in order to evaluate the impact of high-frequency sampling combined with our editing strategy in order to capture small scale coastal signatures. We will also briefly discuss the influence of MDT on glider-altimetry comparisons.

5.2.1. Impact of the MDT

[60] Table 6 summarizes statistical comparisons of the impact of the MDT in the glider and altimetric SAGC comparisons and shows that when the velocity derived from the MDT is added to the altimetric surface geostrophic velocity anomaly, agreement with the glider SAGC is improved. Indeed the mean difference between the two velocities is strongly reduced for all missions. This reduction is of ~10 cm/s for missions of July 2007, November 2007, and June 2008 while it is ~2 cm/s for the mission of April 2008. Concerning the STD, the use of MDT also enables a decrease in the STD difference for the missions of July 2007 and April 2008.

[61] The improvements in terms of mean difference show that MDT performance is satisfactory for wavelengths >40 km (approximately the length of the November 2007 and June 2008 missions). The smaller spatial scale variations cannot be correctly reproduced and thus well evaluated in term of STD given the spatial smoothing and OI procedures used to build the MDT [cf. *Rio et al.*, 2007].

5.2.2. Impact of Sampling and Editing Strategy

[62] In section 3.1.4, we highlighted that both editing strategy and sampling play key roles in the altimetric velocity calculation, especially in the coastal zone. From Figures 9b and 9c, it follows that altimetric SAGC computed from edited 20 Hz altimetric data shows better agreement with the glider SAGC than when using 1 Hz data. This is especially the case in the 50 km coastal zone where a relative strong BC, observed by glider in July 2007, is also captured with 20 Hz data but not seen with 1 Hz data, while out of this area it is interesting to note that the 1 and 20 Hz velocities are consistent. In April 2008, 20 Hz along-track data show SAGC close to that observed by the gliders, the 1 Hz velocity also reproduces the BC in the coastal zone; however, the current exhibits less amplitude than with the glider and 20 Hz data (10–20 cm/s less). The 1 Hz velocities seem also to underestimate the eddy intensity between 40.1°N and 40.4°N, whereas the 20 Hz data shows a better agreement with the glider SAGC. When (M)SLA or standard 42 km smoothed 1 Hz along-track data are used for comparison with the gliders (not shown) the results are worse due to too much spatial smoothing.

[63] From these previous examples, it appears that the 20 Hz altimetric data associated with an adapted editing strategy can recover more data close to the coast and also produce better constraints on coastal altimetric SAGC computations.

6. Conclusions and Perspectives

[64] In the present study, we analyzed the compatibility between glider and altimetry measurements in view of developing an integrated coastal observing system. Altimetric data have been specifically processed to assess a new methodology dedicated to glider SAGC computation. This approach also provided interesting insights into the present limitations and potential improvements of coastal altimetry. The analysis was two-way, using altimetry in support to the glider velocity processing and glider measurements in support of coastal altimetric techniques. We believe that such an approach is necessary before undertaking multisensor data fusions or applications aiming at a quantitative understanding of coastal physical processes.

[65] As a first conclusion, we have shown that simple new processing strategies allow us to generate glider and altimetric SAGC with very good agreement (percentage of STD explained >40% over spatial scales of 20 km). For the glider data set, the importance of the reference level and synopti-

Figure 9. Glider versus altimetric across-track 20 km LP-filtered currents (cm/s) for (left) July 2008 and (right) April 2008 missions. From top to bottom: (a) altimetric SAGC derived from edited 20 Hz data (red curve) vs. surface glider CTD current ($Vg_{z=0_{180}}$, thin blue curve), (b) SAGC derived from edited 20 Hz data (red curve) vs. glider SAGC with application of reference level correction (RLC) and high-frequency geophysical correction (HFGC; blue curve), (c) SAGC derived from 1 Hz data (thin pink curve) vs. glider SAGC with application of RLC and HFGC (blue curve).

Table 6. Statistical Comparisons Between Glider (With Application of RLC and HFGC) and Altimetric (20 Hz) SAGC by Using or Not Using the Mean Velocity Derived From the MDT

	Jul 2007			Apr 2008		
	Mean Diff.	STD Diff.	Nov 2007 Mean Diff.	Mean Diff.	STD Diff.	Jun 2008 Mean Diff.
No MDT	13.6	2.9	23.2	4.8	8.6	9.5
MDT	3.5	1.4	13.9	2.8	7.8	0.7

city issues, due to baroclinic short timescale signals, have been confirmed, whereas Ekman and the high-frequency barotropic component show marginal impacts in our case studies. For altimetry, the use of MDT improve the spatial consistency between the altimetric and glider SAGC despite a lack of spatial resolution that could entail an underestimation of the mean circulation. The use of edited 20 Hz rather than standard 1 Hz and (M)SLA altimetry allows us to go closer to the coast, to increase altimetry-glider agreement and to keep physical signals otherwise eliminated. The main benefit of using 20 Hz data lies more in the greater quality control procedure possibilities with more data, than in spatial scale resolving, given that a 20 km LP filtering is applied.

[66] The combined use of altimetry and glider is promising, allowing observation of coherent general characteristics of the circulation in the Balearic Sea both at the surface and for the whole 180 m water column. High-resolution hydrographic fields from glider and altimetry have revealed the presence of permanent BC and NC signals and non-permanent signals, such as the relatively strong anticyclonic eddy intercepted in April 2008. The synoptic view from remote sensing during the glider missions also suggested a more detailed picture of the mesoscale structures that may play a key role in the exchanges and transport of heat and other biogeochemical properties across the basin. The anticyclonic eddies observed during these missions confirm past studies such as the work of *Pascual et al.* [2002]. This raises the need to quantify the recurrence of such structures that do not appear in the standard circulation scheme but that have impacts on the general circulation in the Mediterranean. Thus, the use of altimetry in combination with gliders could play a major role in revising the general pattern and better characterizing the associated forcing of the Balearic Sea circulation.

[67] As a general conclusion, this study highlights the need for high-resolution coastal measurements made possible thought the development of synergic approaches and the combined use of observing systems at several spatial/temporal scales. Future works could evaluate and compare velocities derived from new coastal altimetric products (PISTACH, COASTALT, etc.) with glider velocities following the approach described in this paper. On a longer term, the Surface Water and Ocean Topography (SWOT) mission can provide very valuable information, complementary to in-situ measurement, for monitoring mesoscale and submesoscale coastal processes. In a more general framework, we believe that multisensor approaches, combining complementary in-situ and remote sensing, will contribute to a better understanding of physical and multidisciplinary processes within the coastal domain. In combination with modeling, multisensor data can significantly help to quantify changes in coastal systems, to comprehend the mechanisms that regulate them, and to forecast their evolution.

Notation

$DH_{z_{180}}$ dynamic height derived from the glider conductivity-temperature-depth (CTD) profile at depth = z meters (with a reference level at 180 m); also refer to Figure 6.

Vg_{abs} surface absolute geostrophic current (SAGC).

$Vg_{z_{180}}$ glider CTD current: cross-track baroclinic component of geostrophic velocity derived from the glider CTD profile at depth = z meters (with a reference level at 180 m); also refer to Figure 6.

$\overline{V_{\mathrm{abs}}}$ glider GPS current:180 m depth average absolute velocity derived from glider GPS positions; also refer to Figure 6.

[68] **Acknowledgments.** We deeply acknowledge the valuable contribution of M. Martínez-Ledesma and B. Casas during the data acquisition phase of the glider missions. Special thanks are also due to B. Garau for processing glider data, to E. Heslop for valuable editing comments, and to R. Escudier and L. Carrère for providing the Ekman and barotropic currents, respectively. The altimeter data were produced by Ssalto/Duacs and distributed by Aviso with support from CNES. Sea surface temperature images were acquired and processed by EUMETSAT. This work has been partially funded by the CICYT-funded projects COOL (CTM2006-12072/MAR) and ECOOP (CTM 2007-31006-E) and by EU-funded projects FP6 ECOOP and FP7 MyOcean.

References

Anzenhofer, M., C. K. Shum, and M. Rentsh (1999), Coastal altimetry and applications, *Tech. Rep.*, *464*, Geod. Sci. and Survey., Ohio State University, Columbus.

Bethoux, J. P. (1980), Mean water fluxes across sections in the Mediterranean Sea, evaluated on the basis of water and salt budgets and of observed salinities, *Oceanol. Acta*, *3*, 79–88.

Birol, F., M. Cancet, and C. Estournel (2010), Aspects of the seasonal variability of the Northern Current (NW Mediterranean Sea) observed by altimetry, *J. Mar. Syst.*, *81*, 297–311, doi:10.1016/j.jmarsys.2010.01.005.

Bouffard, J., S. Vignudelli, P. Cipollini, and Y. Menard (2008), Exploiting the potential of an improved multimission altimetric data set over the coastal ocean, *Geophys. Res. Lett.*, *35*, L10601, doi:10.1029/2008GL033488.

Bouffard, J., L. Roblou, F. Birol, A. Pascual, L. Fenoglio-Marc, M. Cancet, R. Morrow, and Y. Ménard (2010), Introduction and assessment of improved coastal altimetry strategies: Case study over the northwestern Mediterranean Sea, in *Coastal Altimetry*, edited by S. Vignudelli et al., chap. 12, Springer, New York, in press.

Carrère, L., and F. Lyard (2003), Modeling the barotropic response of the global ocean to atmospheric wind and pressure forcing: Comparisons with observations, *Geophys. Res. Lett.*, *30*(6), 1275, doi:10.1029/2002GL016473.

Cipollini, P., et al. (2010), The role of altimetry in coastal observing systems, in *Proceedings of OceanObs'09: Sustained Ocean Observations and Information for Society*, vol. 2, edited by J. Hall, D. E. Harrison, and D. Stammer, *Eur. Space Agency Publ.*, WPP-306, in press.

Cleveland, W. S., and S. Devlin (1988), Locally weighted regression: An approach to regression analysis by local fitting, *J. Am. Stat. Assoc.*, *83*, 596–610.

Durand, F., D. Shankar, F. Birol, and S. S. C. Shenoi (2008), Estimating boundary currents from satellite altimetry: A case study for the east coast of India, *J. Oceanogr.*, *64*, 831–845, doi:10.1007/s10872-008-0069-2.

Durand, F., D. Shankar, F. Birol, and S. S. C. Shenoi (2010), Spatio-temporal structure of the East India Coastal Current from satellite altimetry, *J. Geophys. Res.*, *114*, C02013, doi:10.1029/2008JC004807.

Ekman, V. W. (1905), On the influence of the Earth's rotation on ocean-currents, *Ark. Mat. Astron. Fys.*, *2*(11), 1–52.

Escudier, R. (2009), Estimating surface ocean currents using a multisensor approach, in *Internship Report of ENSTA Engineering School*, edited by A. Pascual and J. Bouffard, Institut Mediterrani d'Estudis Avançats, Mallorca, Spain.

Font, J. (1990), A comparison of seasonal winds with currents on the continental slope of the Catalan Sea (northwestern Mediterranean), *J. Geophys. Res.*, *95*(C2), 1537–1546.

Font, J., J. Salat, and J. Tintoré (1988), Permanent features of the circulation in the Catalan Sea, *Oceanol. Acta*, *9*, 51–57.

Gomis, D., S. Ruiz, and M. A. Pedder (2001), Diagnostic analysis of the 3D ageostrophic circulation from a multivariate spatial interpolation of CTD and ADCP data, *Deep Sea Res., Part I*, *48*, 269–295, doi:10.1016/S0967-0637(00)00060-1.

Hodges, B. A., and D. M. Fratantoni (2009), A thin layer of phytoplankton observed in the Philippine Sea with a synthetic moored array of autonomous gliders, *J. Geophys. Res.*, *114*, C10020, doi:10.1029/2009JC005317.

Jordi, A., G. Basterretxea, and S. Anglès (2009), Influence of ocean circulation on phytoplankton biomass distribution in the Balearic Sea: Study based on sea-viewing wide field-of-view sensor and altimetry satellite data, *J. Geophys. Res.*, *114*, C11005, doi:10.1029/2009JC005301.

La Violette, P. E., J. Tintoré, and J. Font (1990), The surface circulation of the Balearic Sea, *J. Geophys. Res.*, *95*, 1559–1568.

Le Traon, P.-Y., Y. Faugère, F. Hernandez, J. Dorandeu, F. Mertz, and M. Ablain (2003), Can we merge Geosat follow-on with TOPEX/Poseidon and ERS-2 for an improved description of the ocean circulation?, *J. Atmos. Oceanic Technol.*, *20*, 889–895.

Le Traon, P.-Y., and F. Ogor (1998), ERS-1/2 orbit improvement using TOPEX/POSEIDON: The 2 cm challenge, *J. Geophys. Res.*, *103*(C4), 8045–8057, doi:10.1029/97JC01917.

Lueck, R. G., and J. J. Picklo (1990), Thermal inertia of conductivity cells: Observations with a Sea-Bird cell, *J. Atmos. Oceanic Technol.*, *7*, 756–768.

Merckelbach, L. M., R. D. Briggs, D. A. Smeed, and G. Griffiths (2008), Current measurements from autonomous underwater gliders, paper presented at Current Measurement Technology, 2008, 9th Working Conference on Current Measurement Technology, Inst. of Electr. and Electr. Eng., New York.

Morison, J., R. Andersen, N. Larson, E. D'Asaro, and T. Boyd (1994), The correction for thermal-lag effects in Sea-Bird CTD data, *J. Atmos. Oceanic Technol.*, *11*, 1151–1164.

Onken, R., A. Alvarez, V. Fernandez, G. Vizoso, J. Tintore, P. Haley, and E. Nacini (2008), A forecast experiment in the Balearic Sea, *J. Mar. Syst.*, *71*, 79–98, doi:10.1016/j.jmarsys.2007.05.008.

Pascual, A., B. Buongiorno Nardelli, G. Larnicol, M. Emelianov, and D. Gomis (2002), A case of an intense anticyclonic eddy in the Balearic Sea (western Mediterranean), *J. Geophys. Res.*, *107*(C11), 3183, doi:10.1029/2001JC000913.

Pascual, A., D. Gomis, R. L. Haney, and S. Ruiz (2004), A quasigeostrophic analysis of a meander in the Palamós canyon: Vertical velocity, geopotential tendency, and a relocation technique, *J. Physical Oceanogr.*, *34*, 2274–2287.

Pascual, A., C. Boone, G. Larnicol, and P. Y. Le Traon (2009), On the quality of real-time altimeter gridded fields: Comparison with in situ data, *J. Atmos. Oceanic Technol.*, *26*, 556–569, doi:10.1175/2008JTECHO556.1.

Pinot, J. M., J. Tintore, and D. Gomis (1994), Quasi-synoptic mesoscale variability in the Balearic sea, *Deep Sea Res., Part, 1*, *41*, 897–914, doi:10.1016/0967-0637(94)90082-5.

Pinot, J. M., J. L. López-Jurado, and M. Riera (2002), The CANALES experiment (1996-1998). Interannual, seasonal, and mesoscale variability of the circulation in the Balearic Channels, *Prog. Oceanogr.*, *55*, 335–370, doi:10.1016/S0079-6611(02)00139-8.

Poulain, P. M., R. Gerin, E. Mauri, and R. Pennel (2009), Wind effects on drogued and undrogued drifters in the eastern Mediterranean, *J. Atmos. Oceanic Technol.*, *26*, 1144–1156.

Powell, B. S., and R. R. Leben (2004), An optimal filter for geostrophic mesoscale currents from along-track satellite altimetry, *J. Atmos. Oceanic Technol.*, *21*, 1633–1642.

Pujol, M. I., and G. Larnicol (2005), Mediterranean Sea eddy kinetic energy variability from 11 years of altimetric data, *J. Mar. Syst.*, *58*, 121–142, doi:10.1016/j.jmarsys.2005.07.005.

Ray, R. D. (1998), Spectral analysis of highly aliased sea-level signals, *J. Geophys. Res.*, *103*(C11), 24,991–25,003, doi:10.1029/98JC02545.

Rio, M.-H., and F. Hernandez (2003), High-frequency response of wind-driven currents measured by drifting buoys and altimetry over the world ocean, *J. Geophys. Res.*, *108*(C8), 3283, doi:10.1029/2002JC001655.

Rio, M. H., P. M. Poulain, A. Pascual, E. Mauri, G. Larnicol, and R. Santoleri (2007), A mean dynamic topography of the Mediterranean Sea computed from altimetric data, in situ measurements and a general circulation model, *J. Mar. Syst.*, *65*, 484–508, doi:10.1016/j.jmarsys.2005.02.006.

Robinson, A., W. Leslie, A. Theocharis, and A. Lascaratos (2001), Encyclopedia of Ocean Sciences, in *Mediterranean Sea Circulation*, pp. 1689–1706, Academic, London.

Rubio, A., B. Barnier, G. Jordà, M. Espino, and P. Marsaleix (2009), Origin and dynamics of mesoscale eddies in the Catalan Sea (NW Mediterranean): Insight from a numerical model study, *J. Geophys. Res.*, *114*, C06009, doi:10.1029/2007JC004245.

Ruiz, S., A. Pascual, B. Garau, I. Pujol, and J. Tintore (2009a), Vertical motion in the upper ocean from glider and altimetry data, *Geophys. Res. Lett.*, *36*, L14607, doi:10.1029/2009GL038569.

Ruiz, S., A. Pascual, B. Garau, Y. Faugere, A. Alvarez, and J. Tintoré (2009b), Mesoscale dynamics of the Balearic Front, integrating glider, ship and satellite data, *J. Mar. Syst.*, *78*, S3-S16, doi:10.1016/j.jmarsys.2009.01.007.

Ssalto/Duacs (2006), Ssalto/Duacs user handbook: (M)SLA and (M)ADT near-real-time and delayed-time products, *Rep. SALP-MU-P-EA-21065-CLS*, Aviso, Ramonville-Saint-Agne, France.

Tintoré, J., D. P. Wang, and P. E. La Violette (1990), Eddies and thermohaline intrusions of the shelf-slope front off Northeast Spain, *J. Geophys. Res.*, *95*(C2), 1627–1633.

Ursella, L., P.-M. Poulain, and R. Signell (2006), Circulation in the northern and middle Adriatic Sea using surface drifters: Mesoscale to seasonal variabilities, *J. Geophys. Res.*, *111*, C03S04, doi:10.1029/2005JC003177.

Vignudelli, S., P. Cipollini, L. Roblou, F. Lyard, G. P. Gasparini, G. Manzella, and M. Astraldi (2005), Improved satellite altimetry in coastal systems: Case study of the Corsica Channel (Mediterranean Sea), *Geophys. Res. Lett.*, *32*, L07608, doi:10.1029/2005GL022602.

Volkov, D., G. Larnicol, and J. Dorandeu (2007), Improving the quality of satellite altimetry data over continental shelves, *J. Geophys. Res.*, *112*, C06020, doi:10.1029/2006JC003765.

J. Bouffard, A. Pascual, S. Ruiz, and J. Tintoré, Marine Technologies, Operational Oceanography, and Sustainability Department, Mediterranean Institute for Advanced Studies, 21 Miquel Marquès, E-07190 Mallorca, Spain. (jerome.bouffard@uib.es)

Y. Faugère, CLS Space Oceanography Division, 8-10 Hermès, F-31526, Ramonville CEDEX, France.